




REVIEW ARTICLE | AUGUST 14 2025

Toward joint muography and ground deformation monitoring for volcanic unrest assessment

Special Collection: [Muography: Discoveries, Innovations, and Applications](#)






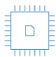
László Oláh   ; Hiroyuki K. M. Tanaka 




J. Appl. Phys. 138, 060701 (2025)

<https://doi.org/10.1063/5.0275038>




 Nanotechnology & Materials Science
  Optics & Photonics
  Impedance Analysis
  Scanning Probe Microscopy
  Sensors
  Failure Analysis & Semiconductors



Unlock the Full Spectrum.
From DC to 8.5 GHz.
Your Application. Measured.

[Find out more](#)



Toward joint muography and ground deformation monitoring for volcanic unrest assessment



Cite as: J. Appl. Phys. **138**, 060701 (2025); doi: [10.1063/5.0275038](https://doi.org/10.1063/5.0275038)

Submitted: 10 April 2025 · Accepted: 22 July 2025 ·

Published Online: 14 August 2025



László Oláh^{1,2,a)} and Hiroyuki K. M. Tanaka^{2,3}

AFFILIATIONS

¹International Virtual Muography Institute (VMI), Tokyo, Japan

²HUN-REN Wigner Research Centre for Physics, Budapest, Hungary

³Earthquake Research Institute, The University of Tokyo, Tokyo, Japan

Note: This paper is part of the Special Topic on Muography: Discoveries, Innovations, and Applications.

a) Author to whom correspondence should be addressed: olah.laszlo@wigner.hun-ren.hu

ABSTRACT

Muography is a geophysical monitoring technique that allows passive, remote, and high-definition density imaging of volcanoes by measuring the yield of penetrated cosmic-ray-induced muon particles. This review focuses on joint muon and ground surface deformation monitoring of active volcanoes and its application for exploring the structures of upper plumbing systems, characterizing the eruptive activities, and contributing to intermediate-term (multi-month) hazard assessment. Our work is based on the data acquired at the active Sakurajima volcano in Japan by the Sakurajima Muography Observatory and synthetic aperture radar. An inverse correlation was found between the muographically measured densities through the conduits of the adjacent craters, suggesting a branched linkage between these conduits. The muographically measured densities were related to the vertical ground surface displacements and monthly number of eruptions and gas emission rates. Periods of low eruption frequency were associated with the formation of a dense plug in the conduit, which caused the inflation of the edifice by trapping pressurized magmatic gas and increased mass density. Periods of high eruption frequency were associated with the release of volcanic gases that caused the deflation of the volcanic edifice and decrease in the mass density. Muography can be utilized to explain the linkage between ground surface deformation and eruptions by revealing the causal physical mechanism. The volcanic unrest index was determined using mass density, vertical displacement, and gas flux data monitored from September 2018 to July 2023. Minor unrest was quantified from September 2019 to December 2020.

© 2025 Author(s). All article content, except where otherwise noted, is licensed under a Creative Commons Attribution (CC BY) license (<https://creativecommons.org/licenses/by/4.0/>). <https://doi.org/10.1063/5.0275038>

I. INTRODUCTION

Forecasting the location, magnitude, duration, and time of impending volcanic eruptions is a key task in applied volcanology.¹ Integrated processing of geophysical, petrological, and geochemical signals may elucidate subsurface volcanic phenomena and improve volcanic hazard assessment.² Ground surface deformation monitoring has revealed pre-eruptive inflation³ and syn-eruptive deflation⁴ of active volcanoes. Nowadays, satellite-based synthetic aperture radars routinely measure the ground surface displacements on active volcanoes every few days.⁵ Synthetic aperture radar (SAR) is even applicable to inaccessible and unmonitored volcanic edifices. Compilation of SAR data acquired at 198 volcanoes showed that just about half of deformed volcanoes erupted, and about one out

of ten non-deformed volcanoes erupted.⁶ These results emphasized that the interpretation of ground deformation monitoring signals relies on correlation and the necessity for applying complementary techniques to elucidate the causative volcanic phenomena before the onset of eruptions. Monitoring of the signals induced by the evolution and movement of magmatic materials in the conduits by density-sensitive techniques, such as gravimetry⁷ or cosmic-ray muon imaging (muography),⁸ may aid the aforementioned limitations of ground deformation monitoring. Here, we focus on joint SAR and muon imaging.

Cosmic-ray muography allows us to perform passive, remote, and non-destructive imaging of large structures, such as volcanoes.^{8–10} The imaging is based on measuring the directionally dependent flux of cosmic-ray-induced, omnipresent, and highly

14 August 2025 13:24:15

penetrating muon particles arriving across the scanned structures into tracking detectors. Muography produces density images and resolves the internal structure and composition of volcanoes with an unprecedented spatial resolution of a few meters from a safe distance of a few kilometers.¹¹ The implementation of muography as a complementary technique for volcano monitoring is still underway in combination with other techniques for different purposes: (A) monitoring of hydrogeomorphic changes caused by volcanic ejecta deposition, erosion, and lahars on the surface of the edifice;^{12,13} (B) reconstructing conduit and crater structures for modeling of eruptive activities;^{14,15} (C) assessing the structural features and composition of volcanic peaks and lava domes for reconstructing past evolution and conducting structural stability analysis;^{16–21} and (D) monitoring of subsurface hydrothermal activities and magmatic processes.^{22,23} Machine learning was utilized for processing daily muographic images for predicting the occurrence of the eruptions of Sakurajima volcano on the next day, and sensitivities and false rates were achieved around 0.75 and 0.2, respectively.^{24,25} These results are not adequate to integrate this innovative technique into complex forecasting systems due to sparse data sets obtained over relatively short periods. Currently, muography has the potential to contribute to the intermediate-term assessment of volcanic eruption sequences.

Here, we are focusing on Sakurajima volcano, which is an active stratovolcano fed with magma from the Aira caldera located beneath Kagoshima Bay, Japan. Primarily, Vulcanian-type eruptions have occurred from two active craters in recent years, with an eruption frequency ranging from a few dozen to a few hundred eruptions per month.^{26–28} We review how muography is utilized for density imaging of the upper conduits of the Sakurajima volcano month by month and relate densities to measurements of vertical ground surface displacements, the SO₂ gas emission rate, and the eruption frequency to explore the plumbing system and study eruption mechanisms. Section II describes the data collected by muography and SAR and the main steps of the analysis procedure. Section III presents the observational results on the conduit structure, eruption mechanism, and the first trial to identify the periods of unrest. Finally, Sec. IV summarizes our findings and discusses the future perspective of hazard assessment.

II. DATA ACQUISITION AND PROCESSING

A. Density monitoring with muography

Muographic data were acquired at the Sakurajima Muography Observatory (SMO) for this study. The SMO is a modular infrastructure that is partly operated with ten multi-wire proportional chamber-based muographic observation systems (MMOSs) by HUN-REN Wigner RCP and the University of Tokyo. The tracking systems, their operational performance, and the power and gas supply systems have been described in detail in previous papers.^{13,14,29–32} Figure 1 shows the topographic map of Sakurajima volcano³³ with the measurement setting. The SMO (O) is operating at a latitude of 31.557°N and a longitude of 130.650°E at a distance of about 2.8 km in the southwest direction from the two craters of Minamidake (A and B) and the Showa (S) crater. The azimuthal orientation of the MMOS is set to 30.25° from north (defined as $\tan(\theta_x) = 0$). Each tracking system is set horizontally (defined as \tan

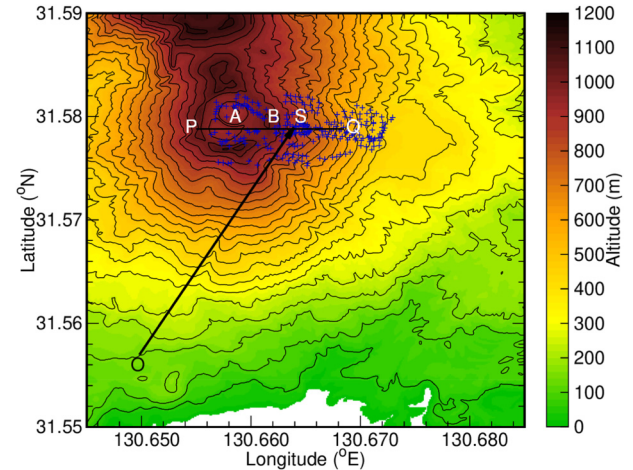


FIG. 1. A topographic map of Sakurajima volcano is shown with the experimental setting. The letter O indicates the location of SMO at a latitude of 31.557°N and a longitude of 130.650°E. The black arrow indicates the orientation of the MMOS. Locations of vertical ground surface displacement measurements are shown with blue crosses. The PQ line shows a slice that was selected across the crater region. The letters A, B, and S correspond to craters Minamidake A, Minamidake B, and Showa, respectively.

($\theta_y = 0$). The data presented here were collected from 1 September 2018 to 1 July 2023. The data acquisition was interrupted for a few days biannually when the MMOS was stopped for maintenance work and installation of new detectors.

The main steps of muographic data processing are presented in Refs. 13 and 34 and are just overviewed hereafter in a nutshell. Quality assurance of the data was conducted by offline analysis. Periods with low-quality data (e.g., malfunctioned electronics and detectors) were excluded from the analysis. Analysis of data acquired by independent MMOS modules built up from the following steps: As a first step, offline alignment of tracking layers and exclusion of malfunctioned electronic channels were conducted by a pre-analysis of a smaller data sample (a few thousand events). The event-by-event analysis was initiated by reconstructing muon hit clusters by quantifying their numbers, sizes, and centroids on each tracking layer in both horizontal and vertical directions. Thereafter, a combinatorial track reconstruction algorithm was applied to measure the track slopes and intercepts. Tracks were counted as a function of horizontal $[\tan(\theta_x)]$ and elevation $[\tan(\theta_y)]$ track slopes. Flux was calculated by dividing the counts by the detector acceptance, solid angle, and measurement time. Muon fluxes measured by independent modules were merged. The density lengths across the edifice were derived by forward modeling of muon fluxes through different-density lengths via numerically integrating directional dependent energy spectra of cosmic-ray muons³⁵ from minimal energies, which required the muons to penetrate the given density lengths.³⁶ The densities were determined by dividing the density lengths by the path lengths of muons across the volcano, which were calculated from the digital elevation model of the edifice.

14 August 2025 13:24:15

B. Ground surface deformation monitoring with synthetic aperture radar

Ground surface deformations of the volcanic edifice were measured by the Phased Array type C-band Synthetic Aperture Radar of the Sentinel-1 satellite every 12 days.³⁷ Blind independent protocol was applied for data processing, i.e., the analysis of SAR images was conducted independently by NEC from our muographic data processing in order to minimize the biased interpretation. Vertical displacements of the surface of the volcanic edifice were calculated relative to the vertical positions quantified for the data that were acquired on 31 October 2018 and 6 April 2021. In Fig. 1, the blue-colored crosses indicate the locations where vertical displacements were calculated.

III. OBSERVATIONAL RESULTS

A. Exploring shallow conduit structure with time-sequential muography

Figure 2 shows the density images measured for periods of 6 months through the crater region (black line) of Sakurajima volcano from 1 January 2021 to 31 May 2023.³⁴ Here, the pixel size corresponds to a spatial resolution of about 60 m by 60 m. Black rectangles indicate the designated regions beneath the eastern part of the Minamidake crater (M), beneath the Showa crater (S), and across a reference region (R). Figures 2(n)–2(x) visualize the unification of conduits beneath the regions M and S from February 2022 and continuous slanting toward the east. These observations were found to be consistent with other monitoring data reported by the Japan Meteorological Agency (JMA): (1) Infrared thermal images indicated the geothermal areas in both craters in October 2021³⁸ and in February and October 2022.³⁹ (2) The seismic hypocenters were observed at shallow depths (<400 m) beneath both craters between June and December in 2021,³⁸ when the densities increased through this unified region. (3) After the unification of regions M and S, the eruptive activity switched from the Minamidake crater to Showa crater in June 2023.²⁸ These results suggest a linkage between the conduits of Minamidake and Showa craters.

Arithmetic mean values of the densities were calculated for the regions M, S, and R for quantifying the relation between the densities measured beneath the two craters and relating these densities to other monitoring signals. Figure 3 shows the averaged densities measured beneath the Showa crater as a function of averaged densities measured beneath the Minamidake crater for the entire data collection period.³⁴ Pearson's coefficient was calculated to be -0.52 , which indicates a moderate inverse correlation between the densities. The simultaneous and inverse change in densities through the adjacent conduits suggests a preferential pathway for degassing that is regulated by the changes in the gas pressure. Similar flow dynamics were quantified for fluid transport between tubes with a branched structure.⁴⁰ At Mount Etna, which is a similar multi-vent volcano, simultaneous changes in the eruptive activity and switching of the infrasonic source location,⁴¹ thermal activity,⁴² and tremors⁴³ were observed between the adjacent Bocca Nuova and South East Crater, and a branched conduit structure was inferred. Muography suggested a similar branched conduit structure for the Minamidake and the Showa craters of Sakurajima

volcano. Geochemical analysis of volcanic ejecta samples from the adjacent craters found that the samples are identical,⁴⁴ which is consistent with the muographic observations. Recently, active seismic surveys of Sakurajima volcano have suggested a unified shallow (<400 m) reservoir beneath the active craters, which feed the conduits with magma.⁴⁵

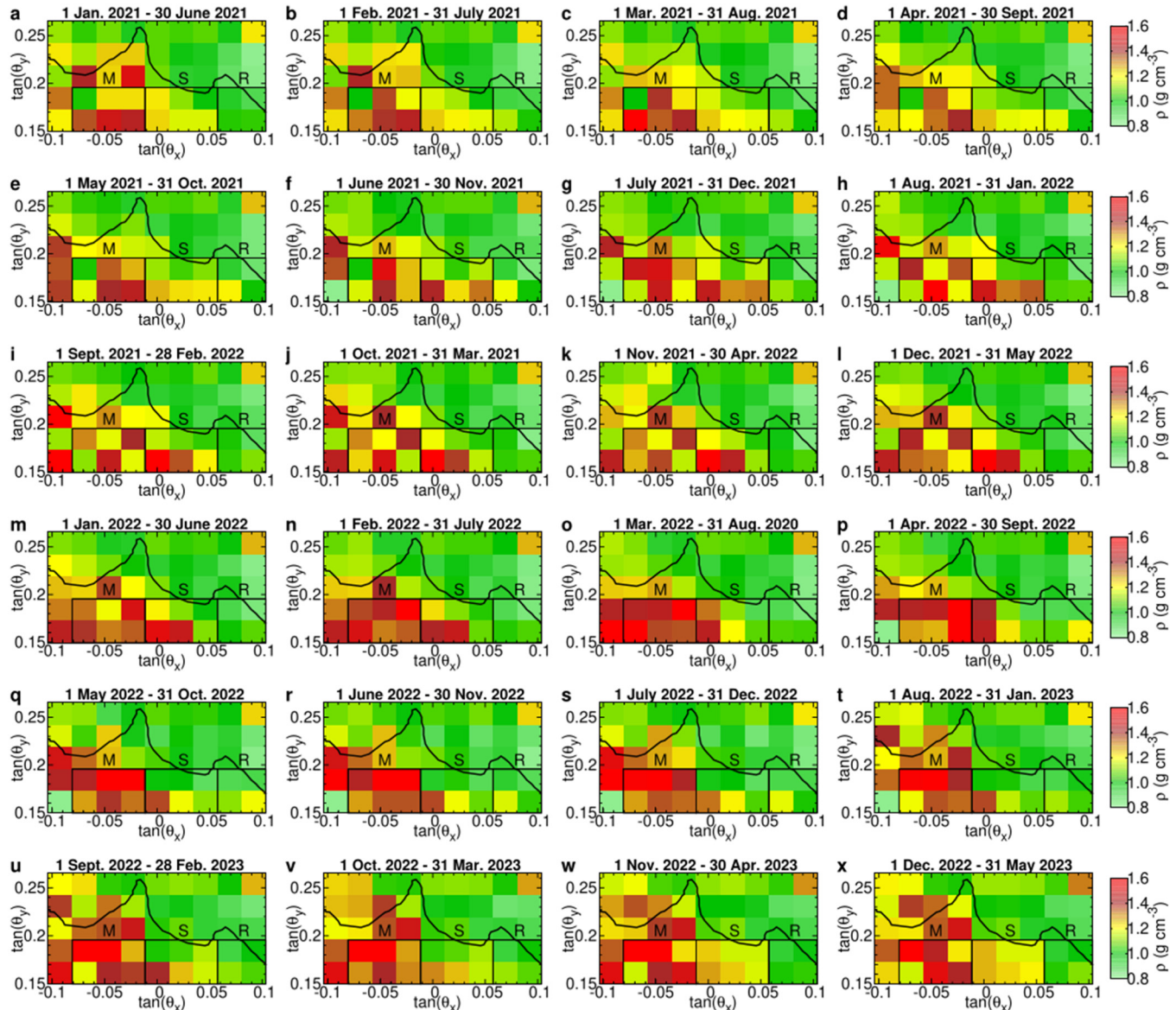
B. In-conduit processes inferred from muon and ground deformation monitoring

Figure 4 shows the time evolution of averaged densities with one standard deviation (black dots with error bars) for the Minamidake crater [Fig. 4(a)], the Showa crater [Fig. 4(b)], and the reference region [Fig. 4(c)] from September 2018 to July 2023.³⁴ The monthly numbers of eruptions are plotted with orange histograms. The colored lines show the vertical displacements measured around the active craters relative to the ground levels determined for 31 October 2018 and 6 April 2021, respectively. The brown dots with error bars show the emission rate of SO_2 gas measured by JMA. As was expected, the density changes were found to be minimal across the reference region in which volcanism did not occur. The observational results and interpretations are discussed for the two active craters in the following paragraphs.

Beneath the Minamidake crater [Fig. 4(a)], the densities increased before the onset of eruptions, and densities decreased during the eruptions. The increase in the density is interpreted as a sign of the formation of a dense magmatic plug in the upper (<200 m from the crater floor) part of the conduit during the periods of low eruption frequency.^{23,46} The inflation of the volcanic edifice during this period is consistent with plug formation driven by pressure from below as the conduit refills with fresh magma. Magma intrusion into the gas pocket may have caused the energetic explosions in June 2020. High-temperature regions and glowing material were observed in the craters. These materials originated from the hot and dense magma plug. The densities correlated with SO_2 emission rates, which is interpreted as density increased as a result of magma degassing. The decrease in the density and vertical displacements during the periods of high eruption frequency is consistent with the presence of gas pockets in the conduit.⁴⁶ The cessation of magma recharge and temporary decrease in the lava level in the conduit may result in the simultaneous deflation of the edifice. The Pearson coefficient was quantified to be -0.66 between the density beneath Minamidake crater and its eruption frequency from October 2019 to May 2021.⁴⁷ As shown in Figs. 4(a) and 4(b), the density increased beneath the Minamidake crater and decreased beneath the Showa crater during the eruptions of the Minamidake crater during the second half of 2022. The cause of material transfer is assumed to be magma movement beneath the active craters toward the east. This material transfer may have caused the weakening of the inverse correlation between eruption frequencies and densities over time. Modeling of the ground deformation source will allow us to track shallow magma movements and explain the change in eruption processes in 2022 and the shift of eruptive activities from the Minamidake crater to the Showa crater in February 2023.

Beneath the Showa crater [Fig. 4(b)], the density increased in January 2019 and in August 2021 due to uprising magma.

14 August 2025 13:24:15



14 August 2025 13:24:15

FIG. 2. The density images of Sakurajima volcano. (a)–(x) The densities (ρ) are visualized as a function of horizontal and elevation directions with slope bin widths of 0.023×0.023 . Each image date was acquired during a period of 6 months. Black rectangles show the studied regions beneath the Minamidake crater (M), the Showa crater (S), and the reference region (R). The black lines show the shape of the craters along the PQ line of Fig. 1. Reproduced with permission from Oláh *et al.* JGR Solid Earth **129**, e2023JB028514 (2024). Copyright 2024 Author(s); licensed under a Creative Commons Attribution (CC BY) license.³⁴

Contrary to the Minamidake crater, the consecutive density decrease was not associated with eruptive activities at the Showa crater. Here, the gas pressure was not sufficient beneath the plug to break it. The decrease in the density is interpreted as bubble formation by convective magma degassing in the conduit.⁴⁸ After plug formation, the surface of the volcanic edifice around the crater was not significantly heightened, indicating the lower pressure gas

beneath the plug. The SAR data indicates that later, the gas pressure increased beneath the plug and reached a sufficient level to trigger eruptions from February 2023. We have to note that volcanic phenomena occurred in the conduit of the Minamidake crater, but the inflation of the Showa crater was also observed. This effect is observed due to the lateral pressure caused by the enlargement and movement of the deformation source.

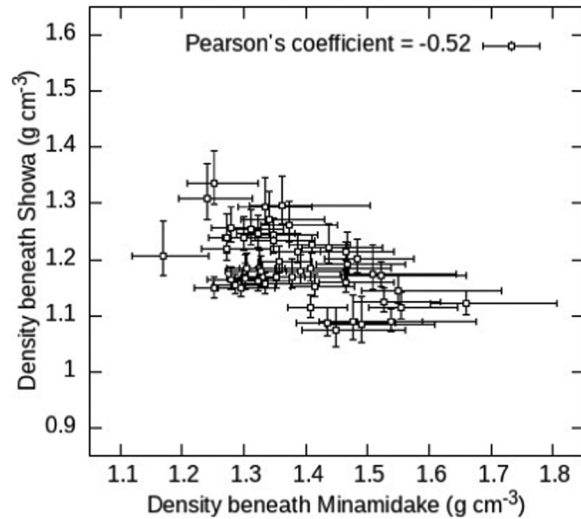


FIG. 3. A scatterplot of mass density values with 1 standard deviation error bars measured beneath the adjacent Minamidake and Showa craters is shown.³⁴ A moderate inverse correlation was quantified between the density values with a Pearson coefficient of -0.52 . Oláh *et al.*, JGR Solid Earth **129**, e2023JB028514 (2024). Copyright 2024 Author(S); licensed under a Creative Commons Attribution (CC BY) license.

C. Assessing unrest level using volcanic unrest index

The volcanic unrest index (VUI)⁴⁹ has been introduced for the semi-quantitative rating of unrest intensity relative to the past level of unrest. The unrest is defined as a level of volcanic activity at a given time relative to the level of activity usually observed. The VUI is not an eruption forecasting tool itself; rather, it helps to communicate the complex and large sets of monitoring data to the society, and it provides input to hazard assessment, specifically to event tree models that are applied for hazard level assessment. Five indices are defined for VUI: 0 for no unrest, 1 for negligible unrest, 2 for minor unrest, 3 for moderate unrest, and 4 for heightened unrest. The indices are quantified by the integer part of the arithmetic mean of indices determined for local earthquake data, local deformation data, geothermal systems, and degassing data.^{49,50}

Here, we utilized the monthly muographic data measured beneath Minamidake crater, the SAR data measured around Minamidake and Showa craters, and the JMA's gas measurement data collected at both of the craters to quantitatively interlink the mass density rate, the vertical ground displacement rate, and the SO_2 gas discharging rate observed from September 2018 to July 2023. Table 1 shows the VUI table of this selected period. In this table, minor unrest (VUI 2) was set when the three kinds of monitoring data rates increased to maximum (September 2019–December 2020). VUI 2 is associated with the period during which the eruption frequency was observed to be the highest.

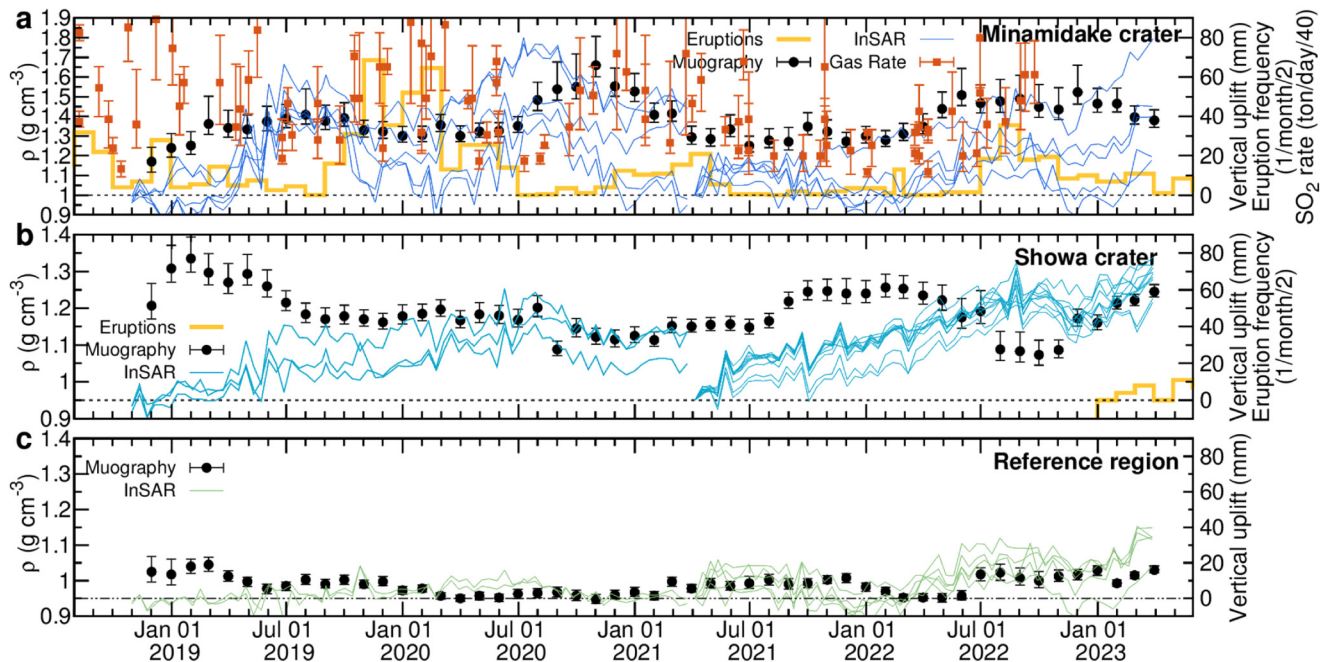


FIG. 4. The average densities are quantified for the selected volumes beneath (a) the Minamidake crater, (b) the Showa crater, and (c) the reference region. The averaged densities (black dots) are plotted for a period between 1 September 2018 and 1 July 2023.³⁴ The dots refer to the middles of six-month periods. The colored lines show the vertical ground surface displacements calculated from data acquired by SAR. The eruption frequencies are shown by orange-colored histograms. The SO_2 emission rates are visualized with brown-colored rectangles with error bars. Oláh *et al.*, JGR Solid Earth **129**, e2023JB028514 (2024). Copyright 2024 Author(s); licensed under a Creative Commons Attribution (CC BY) license.

14 August 2025 13:24:15

TABLE I. The framework of the volcanic unrest index (VUI) was constructed from monitoring data of mass density, vertical ground displacement, and SO₂ gas flux rate for the crater region of Sakurajima volcano from September 2018 to July 2023.

0: no unrest		1: negligible unrest	2: minor unrest
Mass density rate	No change in the density	Low rate of density increase (<0.05 g/cm ³ /month)	Moderate rate of density increase (0.05–0.15 g/cm ³ /month)
Vertical ground displacement rate	No deformation	Low rate of deformation (<10 mm/month)	Moderate rate of deformation (>10 mm/month)
SO ₂ gas flux rate	Low levels of gas flux rate (<1000 t/day)	Moderate levels of gas flux rate (1000–2500 t/day)	Moderate levels of gas flux rate (2500–5000 t/day)

Negligible unrest (VUI 1) and no unrest (VUI 0) were, respectively, set linearly according to VUI 2.

IV. CONCLUSIONS

Muography is a novel geophysical imaging technique that can be applied for passive and remote monitoring of mass density changes across volcanic edifices. Pioneering works have already demonstrated that muography can improve volcano monitoring by resolving the subsurface structure and tracking mass movements beneath active craters with a spatial resolution of a few meters. Implementation of muography in volcanic monitoring systems is still ongoing by combined analysis of data acquired by muography and other techniques, such as gravimetry or seismic noise monitoring, at different volcanoes in the Americas, Asia, and Europe. Here, we focused on muon and ground surface deformation monitoring of the active Sakurajima volcano, Japan. The progress of this approach is summarized and concluded in the following points:^{34,46}

- (1) Time-sequential muography allows us to explore the structure of the upper (typically less than a few hundred meters from the crater floor) part of plumbing systems in multi-vent volcanoes by the visual inspection of density images and quantifying the relation between the average densities measured beneath the adjacent craters.
- (2) Joint analysis of muography and SAR data demonstrated that muography may help to elucidate whether the ground surface inflation is caused by gas pressure increase beneath the magmatic plug due to tectonics and other non-volcanic phenomena or by mass changes associated with magma migration and accumulation. Thus, muography allows the detection and interpretation of pre-eruptive phenomena and makes the correlations between monitoring signals and eruptive activity more robust by linking those via the causal physical mechanism. Muography is expected to improve the models of eruptive processes that affect eruption frequency by physical processes occurring in the upper plumbing system.
- (3) The ground surface displacements were observed as an indirect response to the pressure caused by the deep deformation source. Thus, the regions where the volcanic edifice uplifted were not localized within the size of the deformation source; e. g., volcanic phenomena have occurred in the conduit of one of the two craters, but both craters have upheaved. Thus, the causative processes of volcanic eruptions were localized more accurately by muography than by SAR. We have to emphasize that muography cannot visualize the deep density variations

due to the excessive rock thickness, which is not penetrated by muons over a period of a few months. Muography could explore the upper 120 m of the plumbing system at Sakurajima volcano, and muography rather detected the densification of magmatic materials than the ground deformation source. Forward modeling of ground surface deformations⁵¹ will enable us to track the spatial coordinates and volume change in the ground deformation source and reveal the deeper movement and evolution of the ground deformation source.

- (4) Joint processing of different monitoring data allows us to quantify the volcanic unrest index. Here, we demonstrated the framework of VUI for a shorter period. This procedure will be improved by modeling ground deformation sources, adding earthquake data, and analyzing past events. The VUI will provide a useful input to eruption forecasting models.

Vulcanian-type activity is similar at other volcanoes worldwide (e.g., Semeru, Suwanosejima, and Soufrière Hills),^{26,52} and similar conceptual models can be proposed to describe their eruptive activities. The presented model for intermediate-term changes in the eruptive activity may be applicable to those volcanoes.

ACKNOWLEDGMENTS

This work was supported by the Ministry of Education, Culture, Sports, Science and Technology, Japan (MEXT) Integrated Program for the Next Generation Volcano Research under No. ERI JURP 2025-H-04, of the University of Tokyo, the Hungarian NKFIH research grant under Identification No. TKP2021-NKTA-10, and the HUN-REN Welcome Home and Foreign Researcher Recruitment Programme under No. KSZF-144/2023. Muon detector construction and testing were completed within the Vesztergombi Laboratory for High Energy Physics (VLAB) at HUN-REN Wigner RCP. We acknowledge the useful discussions of Masato Iguchi, Isoji Miyagi, and Edward W. Llewellyn.

AUTHOR DECLARATIONS

Conflict of Interest

The authors have no conflicts to disclose.

Author Contributions

László Oláh: Conceptualization (equal); Formal analysis (lead); Funding acquisition (supporting); Investigation (equal); Software (lead); Visualization (lead); Writing – original draft (lead);

Writing – review & editing (equal). **Hiroyuki K. M. Tanaka:** Conceptualization (equal); Funding acquisition (lead); Investigation (equal); Project administration (lead); Resources (lead); Writing – review & editing (equal).

DATA AVAILABILITY

The data that support the findings of this study are available from the corresponding author upon reasonable request.

REFERENCES

- ¹M. P. Poland and K. R. Anderson, “Partly cloudy with a chance of lava flows: Forecasting volcanic eruptions in the twenty-first century,” *J. Geophys. Res.* **125**, e2018JB016974, <https://doi.org/10.1029/2018JB016974> (2020).
- ²R. S. J. Sparks, J. Biggs, and J. W. Neuberg, “Monitoring volcanoes,” *Science* **335**, 1310–1311 (2012).
- ³D. Patané, P. De Gori, C. Chiarabba, and A. Bonaccorso, “Magma ascent and the pressurization of Mount Etna’s volcanic system,” *Science* **299**, 2061–2063 (2003).
- ⁴D. Massonnet, P. Briole, and A. Arnaud, “Deflation of Mount Etna monitored by spaceborne radar interferometry,” *Nature* **375**, 567–570 (1995).
- ⁵V. Pinel, M. Poland, and A. Hooper, “Volcanology: Lessons learned from synthetic aperture radar imagery,” *J. Volcanol. Geotherm. Res.* **289**, 81–113 (2014).
- ⁶J. Biggs, S. K. Ebmeier, W. P. Aspinall, Z. Lu, M. E. Pritchard, R. S. J. Sparks, and T. A. Mather, “Global link between deformation and volcanic eruption quantified by satellite imagery,” *Nat. Commun.* **5**, 3471 (2014).
- ⁷M. Battaglia and S. Segall, “The interpretation of gravity changes and crustal deformation in active volcanic areas,” *Pure Appl. Geophys.* **161**, 1453–1467 (2004).
- ⁸L. Oláh, H. K. M. Tanaka, and D. Varga, “Muography: Exploring earth’s sub-surface with elementary particles,” *Geophys. Mon. Ser.* **270**, 1–306 (2022).
- ⁹H. Affum, A. Alrheli, A. Darius, S. Andringa Dias, K. Aymanns, D. Barker, C. Besnard-Vauterin, L. Bonechi, G. Bonomi, K. Borozdin, D. Borselli, D. Bosnar, P. Brisset, P. Checchia, E. Cortina Gil, J. Dahlberg, R. D’Alessandro, C. De Sio, C. Díez González, M. Dobrowolska, F. Foulon, A. Giammanco, A. Harel, Y. K. Heng, S. Hlavac, A. Jussofie, R. Kaiser, O. Kamaev, D. Kikola, A. K. H. H. Kopp, J. Marteau, P. Martinez Ruiz Del Arbol, C. Massey, H. Mavric, M. Mhaidra, C. L. Morris, S. Procureur, A. Rezniczek, N. A. Smith, D.-I. Stanca, C. A. Steer, P. Stowell, I. Swainson, L. Thompson, H. Tietze-Jaensch, M. Tytgat, J. Veltius, C. Vieh, M. Weekes, J. Whitlock, G. Yang, and D. Yaish, *Muon Imaging: Present Status and Emerging Applications* (IAEA-TEC-DOC-2012, 2022). <https://www.iaea.org/publications/15182/muon-imaging>.
- ¹⁰H. K. M. Tanaka, C. Bozza, A. Bross, E. Cantoni, O. Catalano, G. Cerretto, A. Giammanco, J. Gluyas, I. Gnesi, M. Holma, T. Kin, I. L. Roche, G. Leone, Z. Liu, D. L. Presti, J. Marteau, J. Matsushima, L. Oláh, N. Polukhina, S. S. V. S. Ramakrishna, M. Sellone, A. H. Shinohara, S. Steigerwald, K. Sumiya, L. Thompson, V. Tioukov, Y. Yokota, and D. Varga, “Muography,” *Nat. Rev. Methods Primers* **3**, 88 (2023).
- ¹¹H. K. M. Tanaka, “Japanese volcanoes visualized with muography,” *Philos. Trans. R. Soc. A* **377**, 20180142 (2019).
- ¹²H. K. M. Tanaka, “Development of the muographic tephra deposit monitoring system,” *Sci. Rep.* **10**, 14820 (2020).
- ¹³L. Oláh, H. K. M. Tanaka, and G. Hamar, “Muographic monitoring of hydrogeomorphic changes induced by post-eruptive lahars and erosion of Sakurajima volcano,” *Sci. Rep.* **11**, 17729 (2021).
- ¹⁴L. Oláh, H. K. M. Tanaka, T. Ohminato, and D. Varga, “High-definition and low-noise muography of the Sakurajima volcano with gaseous tracking detectors,” *Sci. Rep.* **8**, 3207 (2018).
- ¹⁵V. Tioukov, F. Giudicepietro, G. Macedonio, S. Calvari, F. Di Traglia, A. Fornaciai, and M. Favalli, “Structure of the shallow supply system at Stromboli volcano, Italy, through integration of muography, digital elevation models, seismicity, and ground deformation data,” *Geophys. Mon. Ser.* **270**, 75–91 (2022).
- ¹⁶A. Portal, P. Labazuy, J.-F. Lénat, S. Béné, P. Boivin, E. Busato, C. Cârloganu, C. Combaret, P. Dupieux, F. Fehr, P. Gay, I. Laktineh, D. Miallier, L. Mirabito, V. Niess, and B. Vulpesu, “Inner structure of the Puy de Dôme volcano: Cross-comparison of geophysical models (ERT, gravimetry, muon imaging),” *Geosci. Instrum. Methods Data Syst.* **2**, 47–54 (2013).
- ¹⁷R. Nishiyama, S. Miyamoto, S. Okubo, H. Oshima, and T. Maekawa, “3D density modeling with gravity and muon-radiographic observations in Showa-Shinzan lava dome, Usu, Japan,” *Pure Appl. Geophys.* **174**, 1061–1070 (2017).
- ¹⁸M. Rosas-Carbajal, K. Jourde, J. Marteau, S. Deroussi, J. Komorowski, and D. Gibert, “Three-dimensional density structure of La Soufrière de Guadeloupe lava dome from simultaneous muon radiographies and gravity data,” *Geophys. Res. Lett.* **44**, 6743–6751, <https://doi.org/10.1002/2017GL074285> (2017).
- ¹⁹D. Lo Presti, F. Riggi, C. Ferlito, D. L. Bonanno, G. Bonanno, G. Gallo, P. La Rocca, S. Reito, and G. Romeo, “Muographic monitoring of the volcano-tectonic evolution of Mount Etna,” *Sci. Rep.* **10**, 11351 (2020).
- ²⁰G. Macedonio, G. Saracino, F. Ambrosino, G. Baccani, L. Bonechi, A. Bross, M. Bongi, A. Caputo, R. Ciaranfi, L. Cimmino, V. Ciulli, R. D’Alessandro, M. D’Errico, F. Giudicepietro, S. Gonzi, V. Masone, N. Mori, P. Noli, M. Orazi, G. Passeggio, R. Peluso, A. Pla-Dalmau, G. Scarpato, P. Strolin, E. Veretechi, and L. Viliani, “Muography of the volcanic structure of the summit of Vesuvius,” *Geophys. Mon. Ser.* **270**, 123–136 (2022).
- ²¹S. Nagahara, S. Miyamoto, K. Morishima, T. Nakano, M. Koyama, and Y. Suzuki, “Three-dimensional density tomography determined from multi-directional muography of the Omuroyama scoria cone, Higashi-Izu monogenetic volcano field, Japan,” *Bull. Volcanol.* **84**, 94 (2022).
- ²²D. Gibert, J. de Bremond d’Ars, B. Carlus, S. Deroussi, J. Ianigro, D. E. Jessop, K. Jourde, B. Kergosien, Y. Le Gonidec, N. Lesparre, J. Marteau, R. Moretti, F. Nicollin, and M. Rosas-Carbajal, “Observation of the dynamics of hydrothermal activity in La Soufrière de Guadeloupe volcano with joint muography, gravimetry, electrical resistivity tomography, seismic and temperature monitoring,” *Geophys. Mon. Ser.* **270**, 55–73 (2022).
- ²³L. Oláh, H. K. M. Tanaka, T. Ohminato, G. Hamar, and D. Varga, “Plug formation imaged beneath the active craters of Sakurajima volcano with muography,” *Geophys. Res. Lett.* **46**, 10417–10424, <https://doi.org/10.1029/2019GL084784> (2019).
- ²⁴Y. Nomura, M. Nemoto, N. Hayashi, S. Hanaoka, M. Murata, T. Yoshikawa, Y. Masutani, E. Maeda, O. Abe, and H. K. M. Tanaka, “Pilot study of eruption forecasting with muography using convolutional neural network,” *Sci. Rep.* **10**, 5272 (2020).
- ²⁵L. Oláh and H. K. M. Tanaka, “Machine learning with muographic images as input: An application to volcano eruption forecasting,” *Geophys. Mon. Ser.* **270**, 43–54 (2022).
- ²⁶M. Iguchi, H. Yakiwara, T. Tameguri, M. Hendrasto, and J. Hirabayashi, “Mechanism of explosive eruption revealed by geophysical observations at the Sakurajima, Suwanosejima and Semeru volcanoes,” *J. Volcanol. Geotherm. Res.* **178**, 1–9 (2008).
- ²⁷P. Gabellini, R. Cioni, N. Geshi, M. Pistolesi, T. Miwa, G. Lacanna, and M. Ripepe, “Eruptive dynamics and fragmentation mechanisms during cyclic vulcanian activity at Sakurajima volcano (Japan): Insights from ash texture analysis,” *J. Volcanol. Geotherm. Res.* **428**, 107582 (2022).
- ²⁸Japan Meteorological Agency, Monthly number of eruptions of Sakurajima volcano (2025). https://www.jma-net.go.jp/kagoshima/vol/data/skr_erp_num.html.
- ²⁹D. Varga, G. Nyitrai, G. Hamar, G. Galgóczi, L. Oláh, H. K. M. Tanaka, and T. Ohminato, “Detector developments for high performance muography applications,” *Nucl. Instrum. Methods Phys. Res., Sec. A* **958**, 162236 (2020).
- ³⁰D. Varga, G. Hamar, S. J. Balogh, Á. Gera, G. Nyitrai, and G. Surányi, “Construction and readout systems for gaseous muography detectors,” *J. Adv. Instrum. Sci.* **2022**, JAIS-307 (2022).

14 August 2025 13:24:15

- ³¹G. Nyitrai, G. Hamar, and D. Varga, "Toward low gas consumption of muographic tracking detectors in field applications," *J. Appl. Phys.* **129**, 244901 (2021).
- ³²Á Gera, G. Nyitrai, G. Surányi, G. Hamar, and D. Varga, "Gaseous detectors for field applications: Quality control, thermal and mechanical stability," *Instruments* **6**, 74 (2022).
- ³³See <http://www.gsi.go.jp/>. for "Geospatial Information Authority of Japan" (2025).
- ³⁴L. Oláh, G. Hamar, T. Ohminato, H. K. M. Tanaka, and D. Varga, "Branched conduit structure beneath the active craters of Sakurajima volcano inferred from muography," *J. Geophys. Res.* **129**, e2023JB028514, <https://doi.org/10.1029/2023JB028514> (2024).
- ³⁵A. Tang, G. Horton-Smith, V. A. Kudryavtsev, and A. Tonazzo, "Muon simulations for Super-Kamiokande, KamLAND, and CHOOZ," *Phys. Rev. D* **74**, 053007 (2006).
- ³⁶D. E. Groom, N. V. Mokhov, and S. I. Striganov, "Muon stopping power and range tables 10 MeV-100 TeV," *Atomic Data Nucl. Data Tables* **78**, 183–356 (2001).
- ³⁷NEC. See https://www.nec.com/en/global/solutions/space/remote_sensing/index.html for "Remote Sensing Applications, Disaster Monitoring Solutions" (2025).
- ³⁸Japan Meteorological Agency. See https://www.data.jma.go.jp/svd/vois/data/tokyo/STOCK/kaisetsu/CCPVE/shiryo/149/149_2-1.pdf for "Report of 149th coordinating committee of prediction of volcanic eruption" (2021).
- ³⁹Japan Meteorological Agency. See https://www.data.jma.go.jp/svd/vois/data/tokyo/STOCK/kaisetsu/CCPVE/shiryo/151/151_2-1.pdf for "Report of 151th coordinating committee of prediction of volcanic eruption" (2022).
- ⁴⁰M. Manga, "Dynamics of drops in branched tubes," *J. Fluid Mech.* **315**, 105–117 (1996).
- ⁴¹E. Marchetti, M. Ripepe, G. Ulivieri, S. Caffo, and E. Privitera, "Infrasonic evidences for branched conduit dynamics at Mt. Etna volcano, Italy," *Geophys. Res. Lett.* **36**, L19308, <https://doi.org/10.1029/2009GL040070> (2009).
- ⁴²L. Spina, J. Taddeucci, A. Cannata, M. Sciutto, E. Del Bello, P. Scarlato, U. Kueppers, D. Andronico, E. Privitera, T. Ricci, J. Pena-Fernandez, J. Sesterhenn, and D. B. Dingwell, "Time-series analysis of fissure-fed multi-vent activity: A snapshot from the July 2014 eruption of Etna volcano (Italy)," *Bull. Volcanol.* **79**, 51 (2017).
- ⁴³L. Zuccarello, S. De Angelis, V. Minio, G. Saccorotti, C. J. Bean, M. Paratore, and J. M. Ibanez, "Volcanic tremor tracks changes in multi-vent activity at Mt. Etna, Italy: Evidence from analyses of seismic array data," *Geophys. Res. Lett.* **49**, e2022GL100056, <https://doi.org/10.1029/2022GL100056> (2022).
- ⁴⁴A. Matsumoto, M. Nakagawa, M. Amma-Miyasaka, and M. Iguchi, "Temporal variations of the petrological features of the juvenile materials during 2006 to 2010 from Showa crater, Sakurajima volcano, Kyushu, Japan," *Bull. Volcanol. Soc. Jpn.* **58**, 191–212 (2013).
- ⁴⁵T. Nishimura, T. Kozono, A. Matsumoto, M. Nakagawa, and M. Iguchi, "Vulcanian eruptions at Sakurajima volcano: Geophysical data, numerical modeling, and petrological evidence," *Bull. Volcanol.* **86**, 27 (2024).
- ⁴⁶L. Oláh, G. Gallo, G. Hamar, O. Kamoshida, G. Leone, E. W. Llewellyn, D. Lo Presti, G. Nyitrai, T. Ohminato, S. Ohno, H. K. M. Tanaka, and D. Varga, "Muon imaging of volcanic conduit explains link between eruption frequency and ground deformation," *Geophys. Res. Lett.* **50**, e2022GL101170, <https://doi.org/10.1029/2022GL101170> (2023).
- ⁴⁷L. Oláh and H. K. M. Tanaka, "Muography of volcanoes," in *Modern Volcano Monitoring*, edited by Z. Spica and C. Corentin, Advances in Volcanology (Springer Nature, 2025), p. 978-3-031-86840-5.
- ⁴⁸I. Miyagi, H. Shinohara, and J. Itoh, "Variations of color and leachate contents of volcanic ashes from Sakurajima volcano," *Bull. Volcanol. Soc. Jpn.* **58**, 213–226 (2013).
- ⁴⁹S. H. Potter, B. J. Scott, G. E. Jolly, V. E. Neall, and D. M. Johnston, "Introducing the volcanic unrest index (VUI): A tool to quantify and communicate the intensity of volcanic unrest," *Bull. Volcanol.* **77**, 77 (2015).
- ⁵⁰S. H. Potter, B. J. Scott, G. E. Jolly, V. E. Neall, and D. M. Johnston, "A catalogue of caldera unrest at Taupo volcanic centre, New Zealand, using the volcanic unrest index (VUI)," *Bull. Volcanol.* **77**, 78 (2015).
- ⁵¹M. Lisowski, "Analytical volcano deformation source models," in *Volcano Deformation* (Springer Praxis Books, Berlin, 2007).
- ⁵²A. Burgisser, S. Poussineau, L. Arbaret, T. H. Druitt, T. Giachetti, and J.-L. Bourdier, "Pre-explosive conduit conditions of the 1997 vulcanian explosions at Soufrière Hills volcano, Montserrat: II. Overpressure and depth distributions," *J. Volcanol. Geotherm. Res.* **194**, 27–41 (2010).